Experimental Measurements of Irregular Wave Interaction Factors in Closely Spaced Arrays

S. Weller and T. Stallard and P. K. Stansby[1]

[1]Joule Centre, School of Mechanical, Aerospace and Civil Engineering,
The University of Manchester,
PO Box 88, M60 1QD, Manchester, UK
E-mail: Samuel.Weller@postgrad.manchester.ac.uk

Abstract

Much of the published work concerning the response and power output of closely spaced arrays of heaving wave energy devices concerns behaviour in regular waves only and is based on numerical analysis. To date, limited experimental work has been published and it remains unclear how device interactions predicted in idealised models relate to the response of proposed devices in realistic irregular wave-fields. Experimental measurements of the power absorbed by a small two-dimensional array of heaving devices in both regular and irregular waves in a wide flume are reported. Under certain conditions, positive interactions (where the average power output of the array exceeds the same number of isolated devices) are measured. Initial measurements suggest that positive interactions correspond to individual float displacements much larger than the incident wave amplitude. From regular wave tests, the presence of positive interactions is largely dependent on the incident wave period and the performance of adjacent devices. Preliminary tests indicate that float responses tend to be smaller when subjected to short period irregular waves of equivalent peak frequency. The data presented provides an insight into interactions within irregular wave conditions and forms a basis for evaluating numerical models.

Keywords: Interaction factor; Irregular wave; Experimental; Array

Nomenclature

a	=	float radius (m)
a_m	=	measured wave amplitude (m)
β	=	incident wave angle (°)
c_g	=	wave group velocity (m s^{-1})
D_c	=	channel width (m)
f	=	incident regular wave frequency (Hz)
f_p	=	peak frequency of incident irregular wave (Hz)
g	=	acceleration due to gravity (m (s^2)$^{-1}$)
H_s	=	significant wave height (m)
I_{fr}	=	current equivalent to rated torque (mA)
I_{gen}	=	required motor load current (mA)
k_T	=	torque constant (Nm mA^{-1})
L	=	wavelength (m)
l	=	capture width (m)
l_{cm}	=	column averaged capture width (m)
l_{rm}	=	row averaged capture width (m)
m_c	=	counterweight mass (kg)
m_f	=	float mass (kg)
θ	=	angular displacement of float pulley (rad)
P	=	power (W)
q	=	interaction factor
q_{cm}	=	column averaged interaction factor
q_m	=	array averaged interaction factor
q_{rm}	=	row averaged interaction factor
ρ	=	fluid density (kg (m^3)$^{-1}$)
r_p	=	pulley radius (m)
s	=	centre-to-centre spacing (m)
τ_m	=	mechanical torque applied by dynamometer (Nm)
t	=	time (s)
ω_d	=	angular velocity of flywheel (rad s^{-1})
ω_{max}	=	maximum angular velocity of flywheel (rad s^{-1})
ω_{min}	=	minimum angular velocity of flywheel (rad s^{-1})
ω_f	=	angular velocity of float pulley (rad s^{-1})
x	=	long axis of flume (direction of wave propagation)
z	=	vertical axis (positive upward), float displacement (m)

1 Introduction

Arrays of floating bodies supported by a common structure represent one class of wave energy converter (WEC). Although system design details and operation differ, these devices typically consist of multiple floats whose motion in heave is constrained by a power take off system located on a platform above water level. The Fred Olsen FO^3 platform [1] and the Wave Star Energy, Wave Star [2] belong to this category, as does the Manchester Bobber on which the power take off system used in this study is based. In order for any wave energy converter to be commercially viable, it must perform adequately in a range of typical annual wave conditions and must also be sufficiently robust to survive in extreme environments, such as large amplitude waves. This report details small-scale experimental measurements (1:67 geometric scale) of the power capture characteristics of an array of closely-spaced heaving devices with particular focus on net power output due to irregular waves.

1.1 Analysis of Arrays

Theoretical studies based on simplifying assumptions have shown that wave interactions may increase the net power output of an array to be more than from the same number of devices in isolation [3, 4]. To quantify this, an interaction factor (q) equal to unity indicates that the maximum power absorbed is the same as an isolated device, with values greater or less than unity indicating positive and negative interactions.

Budal [5] was perhaps the first to address power absorption from an array of wave energy devices. It was demonstrated that considerable enhancement of power absorption is possible for linear arrays for certain ratios of body spacing to wavelength, assuming that the floating bodies oscillate with equal response amplitude. To ensure this, a pair of connected hemispherical-ended floats (of the same diameter and draft as used in this study but larger spacing, $s = 6.66a$) were used in a water depth of 1.5 m. Budal's experimental work [5] agrees well with point absorber theory in that as the device spacing approaches the wavelength, interaction factor q increases linearly towards π. Similar conclusions were drawn from tests involving an array with larger spacing ($s = 10a$) at the University of Edinburgh (partially reported in [6]). The theory behind this research was relaxed in separate studies by Evans and Falnes [7, 8], who both derived a more general theory for maximising power absorption, the 'point absorber approximation'.

Various numerical studies have quantified the affect of altering incident wave frequency, heading or array layout on interaction factor ([9–11]). Moving away from rectangular array layouts, Fitzgerald and Thomas [11] used nonlinear optimisation techniques to determine optimum array configurations with individual motion constraints based on Thomas and Evans [10]. Budal and Falnes [3, 4] have suggested that a net increase in absorbed power is in fact possible for certain configurations. The findings presented in this study are for one incident wave heading only (β = 0) and fixed device spacing ($s = 4a$), but the apparent balancing mechanism of positive interactions at one wave condition and negative interactions at another is demonstrated in agreement with previous array research. Whilst it would seem that all positive interactions should be exploited for optimum power absorption, research has shown that this would require large device oscillations, far beyond the capabilities of any practicable system design [12]. Instead, McIver [9] suggests that perhaps it is more advantageous to devise wave energy systems that reduce negative interaction effects.

To-date only a few studies have been published concerning the performance of wave energy arrays in irregular waves and most of this analysis has been numerical. Power output smoothing by using arrays of devices have been numerically simulated by Thorburn and Leijon [13] and Tissandier et al. [14]. Whilst this research has collectively generated some important conclusions, such as how the size of the array can affect power output variability, all of the array layouts studied have large device spacings allowing simplification of the analysis by ignoring the influence of device radiation and scattering on interactions. For example the device spacings used in [13], assuming the body radius listed in [15] range from $8a \leq s \leq 32.7a$. Designs of arrays of devices supported by a common structure tend to have a smaller device spacings (around $s = 4a$) for economic and practical reasons, such as high power capture density and ease of maintainability. For these configurations both the radiation force and excitation force differ from that on an isolated body and so must be considered when modelling array response. Response and power output predictions for this type of system have been presented (21 heaving floats analysed using WAMIT by Taghipour and Moan [1]) and spectral summation assumed for irregular waves but the validity of these linear predictions remain unclear. Experimental measurements of the response of an array of five mechanically undamped devices by Thomas et al. [16] have shown that numerical methods based on linear wave forcing and assuming small amplitude response tend to over predict relative float responses near device resonance. Over this range of wave frequencies, measured response ratios ($|z| / |a_{\mathrm{m}}|$) ranged from 1 to 2.5 in a regular wave-field with a full-scale amplitude of 0.86 m. To provide some insight into the behaviour of arrays in realistic wave-fields, this study reports experimental measurements of the power capture of a small rectangular array of 12 (3 x 4) identical devices in both regular and irregular waves. Interaction factors are obtained for both cases to provide a basis for comparison to numerical models.

2 Experimental Equipment

Experimental measurements were carried out in a 5 m wide wave flume with eight Edinburgh Designs wave paddles located 18.5 m from the middle of the beach, Fig 1(a). An individual device located at the centreline of the flume, 2.5 m from the flume side walls and 3.9 m from the wave paddles is used for normalisation of array response measurements. This device is also used as the central drive of the third row in a rectangular array consisting of 12 identical devices separated by centre-to-centre spacing of $s = 4a$. Time varying wave amplitudes (a_{m}) are recorded using seven capacitance-type wave gauges, three of which are shown in Fig 1(a). Wave gauges 5 and 6 (WG5 and WG6), located between the floats and paddles are used to align empty flume measurements (representing the incident wave-field) and populated tank measurements. Wave gauge 4 (WG4) is used for time-varying analysis and is offset to one side of the tank in line with the isolated float position. Wave gauges are calibrated by a series of still water tests over a range of immersion lengths. A constant water depth of 0.46 m is used to represent a full-scale water depth of just over 30 m. All seven wave gauges (and two digital counters per drive, as described below) are monitored at a sample rate of 256 Hz via a National Instruments data acquisition device for an interval of either 48 s or 68 s (for regular and irregular wave tests respectively).

Each 1:67 scale drive system consists of a number of relatively simple mechanical components combined with a custom-made control circuit board. Referring to Fig 1(b) a cable-supported axisymmetric float is held in equilibrium by a counterweight over a pulley. In terms of pulley support, the system is in some respects similar to those reported in [5, 17, 18]. However, unlike these systems a dynamometer is used to compensate for friction and adjust torque during operation. Also the float is permitted to move in surge slightly which eliminates mechanical friction experienced by strut supported systems [19]. Observed horizontal motion is typically less than one radius which is small relative to the cable length. This allows the vertical motion to be approximated using the measured angular pulley displacement and pulley radius such that $z \approx \phi r_p$ with some degree of accuracy. With a float mass equal to m_f = 1.58 kg and counterweight mass equal to m_c = 0.6 kg, the submerged float draft is approximately equal to the float radius a = 0.075 m. This mass combination applies a sufficiently large tension force such that the cable remains taut during the relatively low float accelerations measured during these tests. Other draft settings have been tested by the authors with varying power outputs and float responses [20, 21]. The combination of masses and float draft studied here would be used for typical operating conditions, whilst draft would be reduced in lower sea-states and increased in extreme conditions. The natural period of the system is therefore constant for all tests (approx. 1.2 Hz assuming small amplitude response).

Oscillatory float motions cause the float support pulley to rotate. This shaft is attached to one side of a small sprag clutch which is connected to a high inertia flywheel when engaged. A flexible coupling attached to the other side of the flywheel is also joined to a 12V DC motor. Angular displacement of both shafts (float and drive) are measured using a HEDS9000 quadrature encoder reading an HEDM 6120 T12 code wheel. This provides a displacement measurement resolution of 7.86 x 10 $^{-4}$ rad. If the velocity of the float pulley is equal to that of the drive (i.e. $\omega_f = \omega_d$) then the clutch will engage and flywheel is accelerated due to the force applied by the descending float. As can be seen from the idealised example in Fig 2(b) this occurs in regions 2, 4 and 6. Conversely the clutch will not engage if $\omega_f < \omega_d$ and instead the float response is mechanically unconstrained and the flywheel continues to rotate,

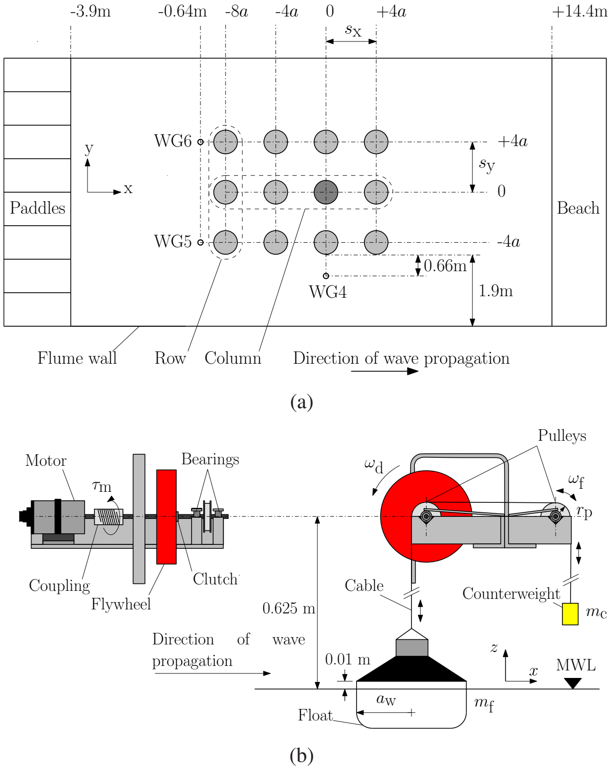

Figure 1: Experimental arrangement of (a) wave flume and (b) front and side views of individual float support indicating float, counterweight, supporting cable, pulley and drive system. Not to scale.

as shown in regions 3, 5 and 7. Unlike some linear drive systems this means that energy is transferred to the flywheel only whilst the float motion is downward. Torque from the motor and friction in the system cause the flywheel to decelerate. The instantaneous power output is therefore directly dependent on drive speed and applied torque ($P = \tau_m \omega_d$).

Measured angular displacements and wave gauges are recorded simultaneously using a 31 channel National Instruments data acquisition device at a rate of 256 Hz. The angular displacement measurements are also taken as input to the control circuit board at a rate of 20 Hz. At each time step, angular drive velocity (ω_d) is calculated using a backward finite difference scheme and this is used to specify the applied torque. Torque is generated using a custom-made dynamometer which provides mechanical damping to counteract flywheel rotation caused by float oscillations. The control circuit board has two operational states which affect how the drive is mechanically damped. During normal operation an assisting current (I_A) is applied, such that $\tau_m = I_A k_T$. Here k_T is a preprogrammed torque constant determined from calibration during drive assembly. The assist current comprises a user-defined motor load (I_{gen}) and a current equivalent to static mechanical friction in the system (I_{fr}). Actual current across the loading motor is monitored by the control circuit board and adjusted continuously to match the target value at a rate of 40 kHz. Absorbed power is defined as the product

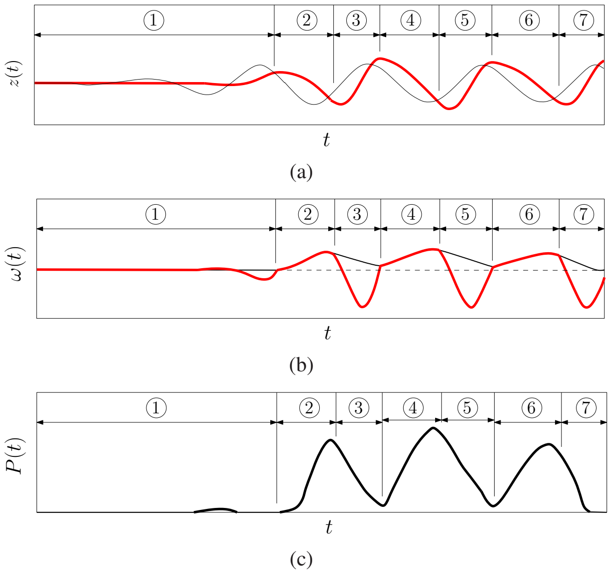

Figure 2: Time-varying idealised example of (a) a low amplitude wave signal (thin black line) and isolated float response (thick red line), (b) a float pulley angular (thick red line) and flywheel (thin black line) velocity signal and (c) an absorbed power signal (thick black line).

of measured speed and applied torque $P = \tau_m \omega_d$. The maximum rated torque is related to the maximum rated power and velocity of the drive $\tau_{max} = P_{max}/\omega_{max}$. For the tests reported in this study, the device is permitted to exceed the maximum rated power for velocities greater than ω_{max}. Referring to Fig 3, a second state is applicable to drive velocities less than the minimum required value ($\omega_d < \omega_{min}$). To avoid stalling the drive, as is almost the case in regions 3, 5 and 7 of Fig 2(b), the assist current is increased linearly until the net torque due to both the drive and the friction in the system is equivalent to the target torque such that $I_A = I_{gen}\omega_d/\omega_{min} + I_{fr}$. In this state, absorbed power is equivalent to $P = \tau_{max}\omega_d^2/\omega_{min}$.

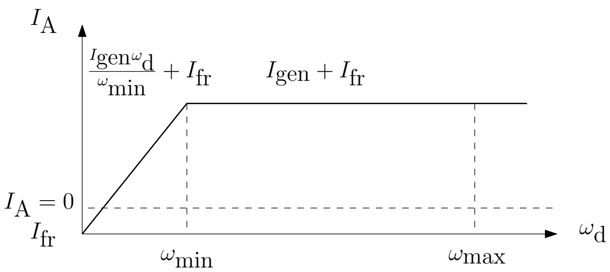

Figure 3: Assist current applied to the loading motor as a function of drive velocity.

After each device has been assembled the mechanical friction in the system is quantified as an equivalent current value and this is used to set the point $I_A = 0$ shown in Fig 3. Friction was not found to vary significantly between tests but some variation may occur over time. To ensure consistency, calibration tests are carried out before each test. Across an array of 12 devices a maximum difference of 34 mA has been noted, equivalent to 83.9 kW full-scale at the rated drive velocity. Several device deceleration tests are carried out from ω_d = 8 to 0 rad/s until an assist current value is found which allows the deceleration to take place over a duration of t = 30 s. The required current load is then offset from the determined assist current value (I_{gen} = 100 mA in this study). Hence, the deceleration gradients of one or more drives are comparable from one test to the other. If used frequently, variation of device friction appears to become negligible.

To provide a summary measure of the performance of a closely spaced rectangular array layout to the same number of isolated devices, interaction factors are calculated for a wide range of scaled incident wave conditions. Small-scale regular waves of amplitudes (a_m) between 0.0075 m and 0.032 m, equivalent to 0.5 m to 2.13 m full-scale with frequencies (f) ranging from 0.5 Hz to 1.63 Hz, equivalent to 16.3 s to 5.0 s full-scale periods are generated. Smith et al. [22] reported that waves of less than 5 s period contribute less than 5% of the annual resource at a typical WEC deployment site. Although ocean conditions are site specific these amplitudes and frequencies represent a broad approximation of operating conditions typical for the system. Based on wave steepness, the wave conditions studied can be modelled using linear theory ($H/L <$ 1/7 for Stokes second-order theory in deep water, where H_s is the significant wave height and L is the wavelength) and represent the range of conditions that are expected to contribute to device power capture. The lower frequency limit of 0.5 Hz satisfies the condition for the full development of a reflected wave-field from a single float; $D_c < L$ where D_c is double the distance between the flume wall and the centreline of the outer floats (4.4 m in still water) and L is the wave length [23]. In the following tests, power output is measured in a range of regular wave conditions and comparison is drawn to measured response in two irregular wave-fields that are defined by a Bretscheider spectrum with equivalent peak frequency and significant wave height to the regular waves. The significant wave heights used are H_s = 0.0376 m and 0.026 m, representing H_s = 2.51 m and 1.73 m full-scale respectively. Surface elevations are also measured without the device in the flume to represent the undisturbed incident wave-field.

3 Measured Float Responses

3.1 Regular Wave Response

Average power values of an isolated device located mid-flume subject to five incident wave amplitudes and 38 frequencies are shown in Fig 4. Within the small-scale regular amplitude and frequency ranges of interest (0.0075 m $< a_m <$ 0.032 m, 0.5 Hz $< f <$ 1.63 Hz) measured regular wave amplitudes appear to vary from required values by -11.9% $< a_m <$ 15.3% and frequencies -0.8% $< f <$ 3.4% using the Hilbert Transform. Because of this variance, the power values

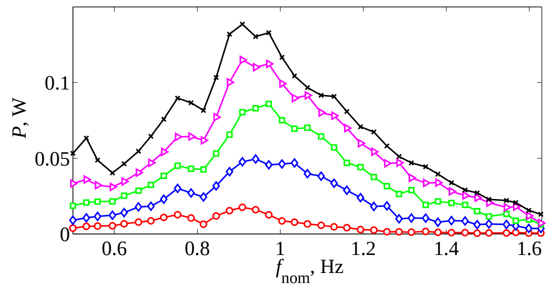

Figure 4: The variation of calculated average power values of an isolated float subjected to regular waves. Nominal amplitude values; a_{nom} = 0.0073 m (red line, circle markers), a_{nom} = 0.014 m (blue line, diamond markers), a_{nom} = 0.0195 m (green line, square markers), a_{nom} = 0.0277 m (magenta line, triangle markers) and a_{nom} = 0.0337 m (black line, cross markers). Power values are averaged over ten float oscillation cycles and are plotted against nominal frequencies f_{nom} averaged from measured values.

in Fig 4 are presented with nominal amplitude and frequency values. Apart from at the highest wave frequency tested, the power absorbed by the device increases with incident wave amplitude as expected. Previous tests by the authors [20] have identified both linear and non-linear float response and wave amplitude regions for an isolated device of the same geometry with a slightly higher natural frequency (1.3 Hz).

Power absorption of the single float varies by -9% $< P <$ 11.5% based on three sets of data measured at seven equispaced frequencies between 0.5 Hz $< f <$ 1.13 Hz and one regular wave amplitude a_m = 0.0188 m. When analysing the power absorption values of the 12 device array, variations of between -4.9% $< P <$ 4.7% were recorded from four sets of irregular wave data at four frequencies and one mean variance. Although the same device for the single device experiments is used in the array layout, the difference in power captured was considerably higher for the regular wave tests (up to 52.5% higher). The float motions of this device may be less chaotic and more predictable due to the presence of other surrounding floats in the array layout.

Non-dimensionalised capture widths for the array of 12 devices are presented in Fig 5. The values are non-dimensionalised by the float radius, $l = P/P_W a$, where $P_W = 0.5\rho g |a_m|^2 c_g$ is the theoretical available wave power based on measured wave amplitudes according to linear wave theory as reported in [9]. Referring to Fig 1(a), row averaged values in Fig 5(a) demonstrate captures widths ranging from $0.09a < l < 0.065a$ of the float radius. These values are well matched for frequencies below $f < 0.688$ Hz. Above this point the similarity between row behaviour disappears, especially at higher frequencies where there is considerable variation. The column averaged values are also well matched in the low and mid frequency ranges, but above $f > 0.938$ Hz lower average capture widths of the central column show reduced performance, possibly due to destructive interferes of radiated waves from the floats located in the outer columns.

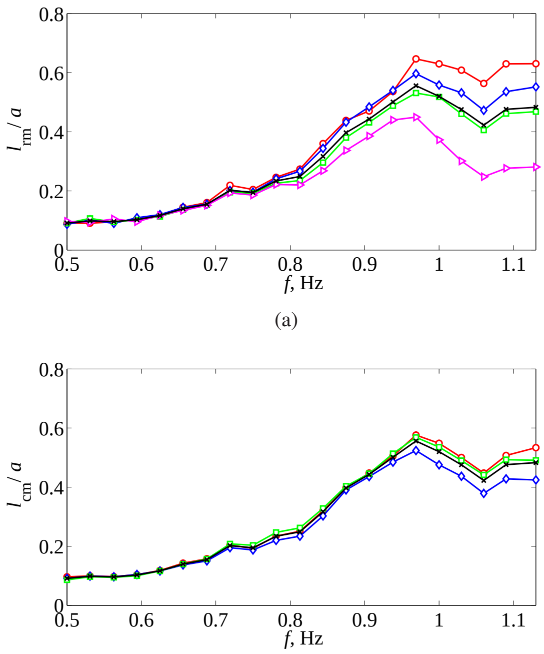

(b)

Figure 5: Calculated (a) row averaged and (b) column averaged non-dimensionalised capture widths of a rectangular array of 12 floats subject to regular waves of amplitude 0.0188 m. First row or column (red line, circle markers), Second row or column (blue line, diamond markers), Third row or column (green line, square markers) and Fourth row (magenta line, triangle markers). For comparison, array averaged values are shown as a solid line with cross markers.

3.2 Regular Wave Interaction Factors

Interaction factors represent a way of assessing the performance of devices in an array layout compared to the same number of identical isolated devices. The ratio of array-based to isolated device power values are calculated for two wave amplitudes (a_m = 0.013 and 0.0188 m) using the isolated values presented in Fig 4. Referring to Fig 1(a), row (q_{rm}) and column (q_{cm}) averaged interaction factors for the array of 12 devices subjected to regular waves are shown in Fig 6(a) and (b). It is clear that most values are close to unity across the frequency range, also shown in both Fig 6(a) and (b) using array averaged values (q_m). For wave frequencies less than $f < 0.781$ Hz there appears to be a distinct lack of order, with the ranking of absorbed power per row dependent on incident wave frequency. Above this point, attenuation of average absorbed power occurs; as the row position moves away from the paddles, progressively less power is absorbed with some values below the array average. Interestingly for high frequencies attenuation across the array becomes more pronounced with increasing frequency. An exception to this appears between 0.906 Hz $< f <$ 0.938 Hz when the second row absorbs marginally more power. For most frequencies

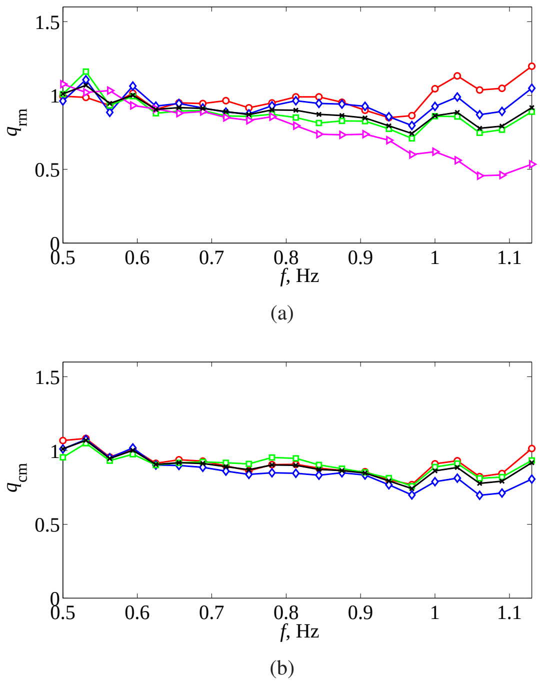

Figure 6: Calculated (a) row averaged and (b) column averaged interaction factors of a rectangular array of 12 floats subject to regular waves of amplitude 0.0188 m. First row or column (red line, circle markers), Second row or column (blue line, diamond markers), Third row or column (green line, square markers) and Fourth row (magenta line, triangle markers). For comparison, array averaged values are shown as a solid line with cross markers.

greater than $f > 0.656$ Hz the central column of devices on average produces less power than the outer columns.

It is likely that the reason for the lack of variation of interaction factors is because the natural frequency of each device (approximately 1.2 Hz) is above the tested range of wave frequencies. If the interaction values in Fig 6 are compared with those from smaller amplitude wave tests (a_m = 0.013 m) in Fig 7, little distinction is apparent across the frequency range. Previous regular waves tests [21] by the authors using the same float geometries, but a different mass combination and so a lower natural frequency (approximately 0.9 Hz) with an additional tethering system, resulted in larger interaction factors. This is apparent if the thick black solid and dashed lines in Fig 7 are compared, which represent an array of 12 floats with high (1.2 Hz) and low (0.9 Hz) natural frequencies subject to waves of amplitude a_m = 0.013 m. The existing results show considerably larger array averaged interaction factors, with a clearly defined peak near $f = 0.781$ Hz and most values close to, or above unity. This array exhibits a resonant response at a frequency less than the natural frequency of the floats. The reduction in interaction factors near $f = 0.938$ Hz is due to the large resonant response of the isolated float in this region.

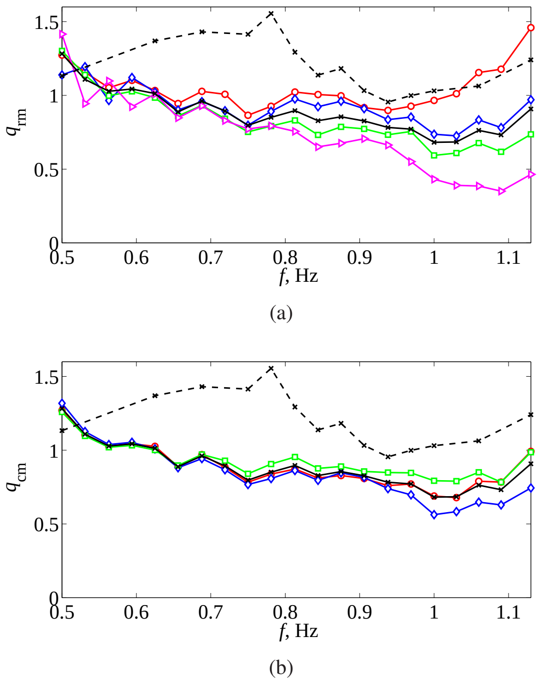

Figure 7: Calculated (a) row averaged and (b) column averaged interaction factors of a rectangular array of 12 floats subject to regular waves of amplitude 0.013 m. First row or column (red line, circle markers), Second row or column (blue line, diamond markers), Third row or column (green line, square markers) and Fourth row (magenta line, triangle markers). For comparison, array averaged values of the high and low natural frequency floats are shown as solid and dashed lines with cross markers respectively.

3.3 Irregular Wave Results

The response of devices subjected to irregular wave spectra with the same peak frequency and significant wave height characteristics as the regular wave conditions reported in the previous Section were also tested. For each peak frequency, average power outputs were calculated over a 64 s interval to include all of the frequency and amplitude components of the spectra. Unlike the regular wave values, clear attenuation occurs (Fig 8(a)) with an almost consistent relationship between the rows across the frequency range. These results suggest a certain degree of fourth row redundancy, although tests with an equivalent array without this row would be required for confirmation. Referring to Fig 8(b) all central devices produce less power than the outer devices on the same row, similarly to the regular wave results. Despite some asymmetry of individual outer devices in the first and fourth rows (up to 12%), the outer column averages are generally well matched across the frequency range.

Analogous row and column averaged trends were recorded at with a lower energy spectrum (H_s = 0.026 m). Row attenuation was still evident for most of the frequency range (above $f_p > 0.531$ Hz), with central column averaged values lower than their outer column counterparts. Differences between the front row and other row values are more noticeable for this wave

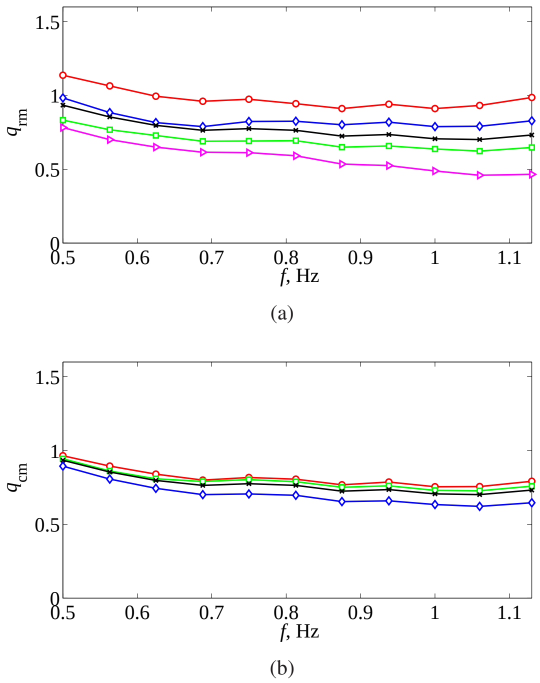

Figure 8: Calculated (a) row averaged and (b) column averaged interaction factors of a rectangular array of 12 floats subject to irregular waves of significant wave height H_S = 0.0376 m. First row or column (red line, circle markers), Second row or column (blue line, diamond markers), Third row or column (green line, square markers) and Fourth row (magenta line, triangle markers). For comparison, array averaged values are shown as a solid line with cross markers.

height condition, with front row interaction factors up to 1.07 at f_P = 0.813 Hz. The array averaged values for each wave spectrum are notably different, unlike the regular wave results. For the entire frequency range the interaction factors associated with the lower significant height are higher. The results from these two wave height cases suggest that destructive interferences due to irregular wave loading increase with wave height. However, further tests at different significant wave heights would be required before firmer conclusions can be drawn.

3.4 Ratio of Power Output in Irregular Waves to Regular Waves

Although irregular wave spectra are more representative of actual sea states than regular wave-fields, the latter are easier to replicate in a small-scale wave flume and can also occur at sea if the peak frequency is sufficiently low. In this Section, the calculated average power outputs of devices subject to irregular and regular wave conditions at one significant wave height (H_S = 0.0376 m) are compared. Fig 9 shows a gradual decline of the ratio between irregular and regular wave power values (P_I/P_R) with increasing peak frequency. Ratios are almost consistently higher for the isolated device case than the array average case. The power captured by a device is typically lower for short period irregular

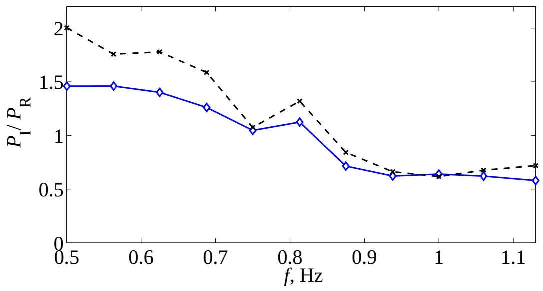

Figure 9: Calculated ratios of averaged power output values of a rectangular array of 12 floats (thick blue line, diamond markers) and isolated device (thick dashed line, cross markers) in irregular and regular waves of equivalent peak frequency and significant wave height H_S = 0.0376 m.

wave conditions than regular wave conditions of equivalent peak frequency and energy spectrum. The opposite is true for long period waves with peak frequencies lower than $f_P = f < 0.875$ Hz. From observation, the low amplitude response of an isolated device or array of devices subject to regular wave spectrum at low frequencies will lead to a lower power output average than that from an irregular wave spectrum.

Time-varying plots of float and flywheel velocity (*top*) and power output (*bottom*) are shown in Fig 10 for an isolated device subject to an irregular wave-field with a peak frequency f_P = 0.5 Hz and significant wave height H_S = 0.0368 m. Close to the start of the sample (between 5.0 s $< t <$ 10.0 s) the irregular and regular wave-field device responses are similar; almost periodic with small float displacements due to small amplitude wave cycles. However, the influence of larger amplitude and higher frequency wave cycles in the irregular wave-field cause larger float motions, higher flywheel velocities and in turn larger average power outputs. Over the entire sample, the regular wave float displacements continue to be close to the incident wave amplitude resulting in consistently low flywheel velocities and power output, as indicated by the thick red dashed line. The difference between the regular wave device response at this peak frequency and the variability of irregular wave device response is more apparent later on in the measured time series, between 40.0 s $< t <$ 45.0 s. During this interval, the device is briefly subject to a few large amplitude irregular wave cycles close to the device natural frequency. The result of this is a short interval of near-resonant float response, enabling the flywheel to accelerate and then leading to continuous power generation as the wave amplitude drops. This, and the fact that the excitation force due to the wave-field and float velocity are almost in phase, are the main reasons for the differences in power output at the lower peak frequencies. When comparing higher peak frequency conditions close to the natural frequency of the system (i.e. $f_P > 1.0$ Hz, see Fig 9), a more resonant regular wave response is observed with float displacements much larger than the incident wave amplitude. This, combined with

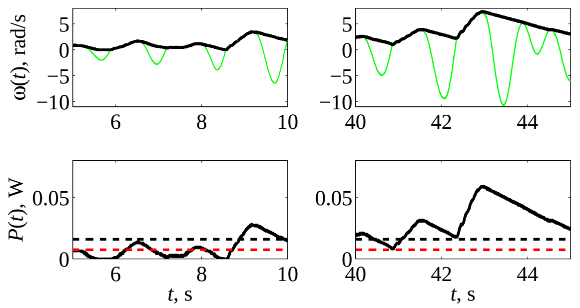

Figure 10: Time-varying velocity (top) and power output (bottom) responses of an isolated device subject to an irregular wave-field (f_p = 0.5 Hz and H_s = 0.0368 m). (*Top*) irregular wave float velocity (thin green line), irregular wave flywheel velocity (thick black line). (*Bottom*) time-varying (thick black line) and time-averaged (thick dashed black line) power output. Also shown is the time-averaged (thick dashed red line) power output of the same device subjected to an equivalent regular wave-field.

the presence of several small amplitude wave cycles in the equivalent irregular wave spectrum, which result in prolonged low flywheel velocities, result in power ratio values (P_I/P_R) below unity.

In summary, good repeatability of the calibrated devices is demonstrated, allowing confidence in using the performance of an isolated device to predict the net output of an array through calculated interaction factors. With increasing wave frequency, array averaged interaction factors decline from approximately q_m = 1.1 to 0.8 in regular waves and q_m = 0.9 to 0.8 in irregular waves of equivalent significant wave height H_s = 0.0376 m. In previous tests, higher mean array power output values were observed for an identical array layout with a lower float natural frequency. Comparisons between the response of devices subjected to regular and irregular wave-fields have shown that time-varying power output is not only dependent on the influence of one incident wave cycle, but also previous wave cycles. Under certain conditions, the power output from an irregular wave-field will be higher than an equivalent regular wave-field due to one or more large wave cycles which cause sustained flywheel and generator rotation. The opposite case is possible if the regular wave response is close to device resonance because of comparatively large variations in irregular wave float response. Whilst the device responses reported here are specific to one system design, ensuring consistency of power output in a range of realistic wave conditions is an important consideration for other WEC developers.

4 Conclusions

The majority of numerical models of array interactions have addressed arrays of relatively large spacing and have generally been limited to idealised response in regular waves. Experimental testing is required for both the development and ultimate verification of such models. Here, the performance of an array of 12 (3 x 4) custom-made heaving wave energy devices are compared with an identical isolated device in a broad range of scaled sea states. Comparisons between the power absorbed by an array of 12 heaving axisymmetric devices and an isolated device have produced interaction factors around unity in regular waves. Row attenuation across the array in the direction of wave propagation is observed in short period waves. A lower array response in analogous irregular waves leads to lower interaction factors, with attenuation and symmetry of the outer devices occurring for the entire frequency range tested. Array averaged interaction factors are relatively constant across the tested frequency range, around 0.95 in regular waves and 0.85 in irregular waves of equal significant wave height (approximately equal to half the float radius) and peak frequency. Calculated interaction factors appear to vary with both incident wave conditions and device location within the array suggesting the existence of both constructive and destructive wave interactions. For the regular wave conditions tested clear differences between the response of each row of the array are only evident at high wave frequencies. Similar power output trends occur for two incident wave heights tested, but array averaged interaction factors are largely incident wave frequency dependent. Here interaction factors above unity have been noted in long period regular waves. Previous tests involving an array (3 x 4) of the same geometry floats, but with a lower natural frequency resulted in both higher power output values and interaction factors over a broader frequency range. Therefore device response appears to be sensitive to float draft.

5 References

Acknowledgements

Financial support for this study was provided by the NWDA Joule Centre for Energy Research. In addition, the first author is supported by a Doctoral Training Award from the University of Manchester and an IMechE Whitworth Senior Scholarship. Discussions with Dr Alan Williamson, Dr Frank Allison (UMIP) and the technical contributions of Robert J. E. Brown of Manchester University are greatly appreciated.

References

[1] R. Taghipour and T. Moan. Efficient frequency-domain analysis of dynamic response for the multi-body wave energy converter in multi-directional waves. In *Proceedings of the 18th International Offshore and Polar Engineering Conference*, Vancouver, Canada, 2008.

[2] A. Bjerrum. The Wave Star Energy concept. In *Proceedings of the 2nd International Conference on Ocean Energy*, Brest, France, 2008.

[3] K. Budal and J. Falnes. *Power from Sea Waves*, chapter Interacting point absorbers with controlled motion, pages 381–399. Academic Press, 1980.

[4] K. Budal and J. Falnes. Wave-power absorption by parallel rows of interacting oscillating bodies. *Applied Ocean Research*, 4(4):194–207, 1982.

[5] K. Budal, J. Falnes, Å. Kyllingstad, and G. Oltedal. Experiments with point absorbers [in regular waves]. In *Proceedings of First Symposium on Wave Energy Utilization*, pages 253–282, Gothenburg, Sweden, 1979.

[6] B. Count. *Wave diffraction by a long array of cylinders*. PhD thesis, The University of Edinburgh, 1980.

[7] D. V. Evans. *Power from Sea Waves*, chapter Some analytic results for two- and three- dimensional wave-energy absorbers, pages 213–249. Academic Press, 1980.

[8] J. Falnes. Radiation impedance matrix and optimum power absorption for interacting oscillators in surface waves. *Applied Ocean Research*, 2:75–80, 1980.

[9] P. McIver. Some hydrodynamic aspects of arrays of wave-energy devices. *Applied Ocean Research*, 16(2):61–69, 1994.

[10] G. P. Thomas and D. V. Evans. Arrays of three-dimensional wave-energy absorbers. *Fluid Mechanics*, 108:67–88, 1981.

[11] C. Fitzgerald and G. P. Thomas. A preliminary study on the optimal formation of an array of wave power devices. In *Proceedings of the 7th European Wave and Tidal Energy Conference*, Porto, Portugal, 2007.

[12] D. V. Evans. Maximum wave-power absorption under motion constraints. *Applied Ocean Research*, 3(4):200–203, 1981.

[13] K. Thorburn and M. Leijon. Farm size comparison with analytical model of linear generator wave energy converters. *Ocean Engineering*, 34(5–6):908–916, 2007.

[14] J. Tissandier, A. Babarit, and A. H. Clément. Study of the smoothing effect on the power production in an array of SEAREV wave energy converters. In *Proceedings of the 18th International Offshore and Polar Engineering Conference*, Vancouver, Canada, 2008.

[15] C. Boström, E. Lejerskog, M. Stålberg, K. Thorburn, and M. Leijon. Experimental results of rectification and filtration from an offshore wave energy system. *Renewable Energy*, 34(5):1381–1387, 2009.

[16] S. Thomas, S. Weller, and T. Stallard. Float response within an array: Numerical and experimental comparison. In *Proceedings of the 2nd International Conference on Ocean Energy*, Brest, France, 2008.

[17] M. Vantorre, R. Banasiak, and R. Verhoeven. Modelling of hydraulic performance and wave energy extraction by a point absorber in heave. *Applied Ocean Research*, 26(1-2):61–72, 2004.

[18] K. Hadano, P. Koirala, K. Nakano, and M. Watanabe. Energy obtained by the float-type wave system. *MTTS/IEEE TECHNO-OCEAN '04*, 4:1867–1874, 2004.

[19] T. Bjarte-Larsson. Friction for a floating body heaving along a fixed vertical guiding strut. In *Proceedings of the 7th European Wave and Tidal Energy Conference*, Porto, Portugal, 2007.

[20] T. Stallard, S. Weller, and P. K. Stansby. Limiting heave response of a wave energy device by draft adjustment with upper surface immersion. *Applied Ocean Research*, In-Review, 2009.

[21] T. Stallard, P. K. Stansby, and A. Williamson. An experimental study of closely spaced point absorber arrays. In *Proceedings of the 18th International Offshore and Polar Engineering Conference*, Vancouver, Canada, 2008.

[22] G. H. Smith and V. Venugopal. A generic study for determining WEC power conversion from a random sea. In *Proceedings of the 16th International Offshore and Polar Engineering Conference*, San Francisco, USA, 2006.

[23] T. Bjarte-Larsson, J. Falnes, and T. Moan. Comparison of results from time-domain simulations and model tests of a water-pumping wave-power unit. In *Proceedings of the 16th International Offshore and Polar Engineering Conference*, San Francisco, USA, 2006.